

Biomolecular System Energetics

Peter J. Gawthrop*¹ and Edmund J. Crampin^{1,2,3}

¹ Systems Biology Laboratory, Department of Biomedical Engineering,
Melbourne School of Engineering, University of Melbourne, Victoria 3010,
Australia.

²School of Mathematics and Statistics, University of Melbourne University of
Melbourne, Victoria 3010, Australia

³School of Medicine, University of Melbourne, Victoria 3010, Australia

February 19, 2021

Abstract

Efficient energy transduction is one driver of evolution; and thus understanding biomolecular energy transduction is crucial to understanding living organisms. As an energy-orientated modelling methodology, bond graphs provide a useful approach to describing and modelling the *efficiency* of living systems. This paper gives some new results on the efficiency of metabolism based on bond graph models of the key metabolic processes: glycolysis.

Contents

1	INTRODUCTION	2
2	MODELLING	3
2.1	Chemical reactions	3
2.2	Numerical Values	4
2.3	Redox reactions	5
2.4	Glycolysis	6
3	EFFICIENCY	8
4	CONCLUSION	10

*Corresponding author. peter.gawthrop@unimelb.edu.au

1 INTRODUCTION

Katchalsky's breakthroughs in extending bond graphs to biochemistry are very much on my own mind. I remain convinced that BG models will play an increasingly important role in the upcoming century, applied to chemistry, electrochemistry and biochemistry, fields whose practical consequences will have a significance comparable to that of electronics in this century.

Henry Paynter, 1993

As noted by Paynter [1], Oster, Perelson, and Katchalsky [2] used bond graphs in their seminal paper *Network Thermodynamics* to describe and analyse systems of coupled chemical reactions. This work was extended by Karnopp [3], Cellier [4], Thoma and Mocellin [5] and Greifeneder and Cellier [6]. These ideas were introduced to the Systems Biology community by Gawthrop and Crampin [7, 8]. As noted by Karnopp [3] the bond graph approach is particularly appropriate to electrochemical systems and therefore can be used to model the bioenergetics of excitable membranes [9, 10], redox reactions and chemiosmotic energy transduction in mitochondria [11].

Organisms need energy to drive essential organs including the brain [12, 13], heart [14, 15] and muscles [16]. As discussed in the text books [17, 18], this energy is derived from metabolism involving glycolysis¹, the TCA cycle² and the mitochondrial³ respiratory chain [19]. Both glycolysis and the mitochondrial respiratory chain produce energy storage molecule ATP (adenosine triphosphate) Energy plays a key role in evolution [20, 21]. In particular, evolutionary pressure would be expected to lead to organisms with both efficient energy production and consumption.

Efficiency of production has been experimentally investigated in the context of glycolysis and the TCA cycle by Park, Rubin, Xu, Amador-Noguez, Fan, Shlomi, and Rabinowitz [22] and in the context of the mitochondrial respiratory chain by Lark, Torres, Lin, Ryan, Anderson, and Neuffer [23]. Efficiency of energy consumption has been considered in the context of neurons by Niven [13], in the context of the heart by Lopaschuk and Dhalla [24], and in the context of muscle by [16]. Feedback systems regulate metabolism and its efficiency Hardie [25], Tran, Loiselle, and Crampin [26], Donati, Sander, and Link [27].

In the context of living systems, efficiency has been defined in a number of ways including ATP/O ratio [23] and thermodynamic definitions consistent with engineering practice [16, 28]. The latter approach is used here.

As discussed by Beard [29] meaningful numerical simulation of living systems requires, *inter alia*, a firm thermodynamic foundation. Such a foundation is especially important in the context of investigating efficiency. As an energy-based modelling approach, the bond graph provides

¹Glycolysis is the metabolic process converting the sugar Glucose to the intermediate high-energy molecule pyruvate.

²The tricarboxylic acid (TCA) cycle, also known as the citric acid cycle or the Krebs cycle, converts the high-energy molecule pyruvate into the high-energy molecule NADH (reduced nicotinamide adenine dinucleotide).

³Mitochondria are organelles within many cells which provide efficient conversion of the products of the TCA cycle into ATP.

a firm foundation for studying living systems in general and biomolecular system energetics in particular.

§ 2 is an introduction to bond graph modelling of biomolecular systems based on the specific system analysed in the paper. § 3 gives a bond graph approach to the efficiency of biomolecular systems illustrated by the example of glycolysis and § 4 concludes the paper.

2 MODELLING

This section introduces the modelling of biomolecular systems using bond graphs using the example of the first stage of human metabolism, glycolysis, which converts the high-energy molecule glucose (GLC) to the high-energy molecule pyruvate (PYR), and also generating adenosine triphosphate (ATP) and (reduced) nicotinamide adenine dinucleotide (NADH). § 2.1 looks at a single reaction: ATP hydrolysis, § 2.2 discusses how the numerical values were obtained and § 2.3 examines *redox* (reduction-oxidation) reactions. § 2.4 discusses the modular bond graph modelling of glycolysis: the first stage of aerobic respiration.

2.1 Chemical reactions

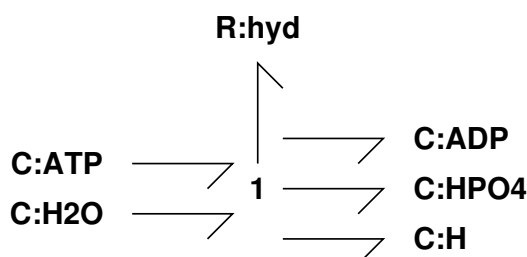


Figure 1: ATP hydrolysis: reaction (1)

The reaction of adenosine triphosphate ATP with water H_2O to form adenosine diphosphate ADP, inorganic phosphate HPO_4^{2-} and a proton H^+ is known as *ATP hydrolysis* and is given by Berg, Tymoczko, and Stryer [30, § 18.4, p.564] as



In bond graph terms, each chemical (ATP, H_2O etc.) can be regarded as a **C** component accumulating each particular chemical and the hydrolysis reaction *hyd* can be regarded as an **R** component driven by the chemical potentials μ_{ATP}, μ_{H_2O} etc. with units of J/mol generating the molar flow v with units of mol/sec. Reaction stoichiometry implies that the molar flow v is out of ATP and H_2O and into ADP, HPO_4 and H. As the the product $\mu \times v$ has units of J/sec, μ and v are covariables. Hence the reaction (1) may be modelled by the bond graph of Figure 1.

As discussed by Gawthrop [11], it is helpful (to engineers) to measure quantity in Coulombs rather than moles and the corresponding conversion factor is Faraday's constant $F = 96\,485 \text{ C mol}^{-1}$.

Noting that $J C^{-1}$ has the special unit Volt (V) and $C s^{-1}$ has the special unit Ampere (A), the effort covariable becomes the *Faraday-equivalent potential* $\phi = F\mu V$ and the flow covariable becomes the *Faraday-equivalent flow* $f = \frac{1}{F}vA$.

Using the standard formula for chemical potential as a function of quantity [31], the *Constitutive Relationship* (CR) of a chemical **C** component associated with substance A gives the potential ϕ_A in terms of the amount x_A in terms of the potential ϕ_A^\ominus and amount x_A^\ominus at standard conditions

$$\phi_A = \phi_A^\ominus + V_N \ln \frac{x_A}{x_A^\ominus} \quad (2)$$

$$= V_N \ln K_A x_a \quad (3)$$

$$\text{where } V_N = \frac{RT}{F} \approx 26 \text{ mV and } K_A = \frac{\exp \frac{\phi_A^\ominus}{V_N}}{x_A^\ominus} \quad (4)$$

The Faraday-equivalent potential ϕ_A° at any other operating point can be computed from Equation (2) as

$$\phi_A^\circ = \phi_A^\ominus + V_N \ln \rho_A \quad (5)$$

$$\text{where } \rho_A = \frac{x_A^\circ}{x_A^\ominus} = \frac{c_A^\circ}{c_A^\ominus} \quad (6)$$

and c_A° and c_A^\ominus are the concentrations at the relevant conditions.

Whereas each *species* A is associated with a *potential* ϕ_A , each *reaction* r is also associated with a *reaction potential* (which is denoted Φ) split into two components: the *forward reaction potential* Φ^f and the *reverse reaction potential* Φ^r . The net reaction potential, which drives the reaction, is given by $\Phi = \Phi^f - \Phi^r$. In the case of the reaction (1)

$$\Phi^f = \phi_{\text{ATP}} + \phi_{\text{H}_2\text{O}} \quad (7)$$

$$\Phi^r = \phi_{\text{ADP}} + \phi_{\text{HPO}_4} + \phi_{\text{H}} \quad (8)$$

$$\Phi = \phi_{\text{ATP}} + \phi_{\text{H}_2\text{O}} - (\phi_{\text{ADP}} + \phi_{\text{HPO}_4} + \phi_{\text{H}}) \quad (9)$$

The CR of a chemical **R** component (assuming mass-action kinetics) is

$$f = \kappa \left(\exp \frac{\Phi^f}{V_N} - \exp \frac{\Phi^r}{V_N} \right) \quad (10)$$

This CR requires the forward (Φ^f) and reverse (Φ^r) potentials separately; as discussed by Karnopp [3] this requires either an implicit modulation or a two-port **R** component.

2.2 Numerical Values

Perhaps surprisingly, values for standard potentials and typical cellular concentrations can be hard to find in the biochemical literature. The values used in this paper come from two sources.

Chemical potentials μ^\ominus at standard conditions are taken from Li, Wu, Qi, and Beard [32, Table 5] and converted to Faraday-equivalent potentials $\phi^\ominus = F\mu^\ominus$. Concentrations are taken Park et al. [22, Table 5] and are used in conjunction with Equation (5) to compute potentials at typical cellular conditions.

Reconciling experimental data is a big issue that is beyond the scope of this paper – see, for example, Tummler and Klipp [33]. Using the aforementioned data, some reactions discussed in § 2.4 were found to have small negative potentials; these are not thermodynamically feasible and so the data from Li et al. [32, Table 5] was modified to give small positive potentials. In particular, the potentials of DHAP and GAP were adjusted by 10 mV, about 0.1%. In general, reaction potentials are the difference of large species potentials and thus small percentage changes in the latter can give large percentage changes in the former.

Under such typical cellular conditions, reaction (1) is associated with a Faraday-equivalent potential Φ of about 532 mV; for this reason the reaction can be used to pump chemical reactions against an adverse potential gradient.

2.3 Redox reactions

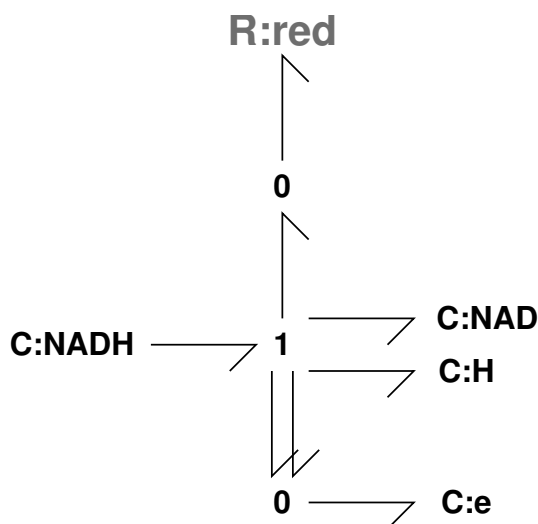
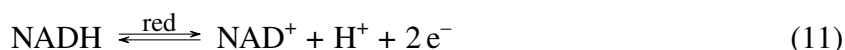


Figure 2: NADH reduction: reaction (11)

Redox (reduction/oxidation) reactions are the key to aerobic life; the bond graph modelling of such reactions is described by Gawthrop [11]. Redox reactions can be split into two half reactions each of which explicitly contains the electrons donated or accepted by the reaction. As an example of this in the first stage of the mitochondrial electron transport chain, NADH (reduced Nicotinamide Adenine Dinucleotide) donates two e^- (electrons) in forming NAD^+ (oxidised Nicotinamide Adenine Dinucleotide) which are accepted by Q (oxidised Ubiquinone) to form QH_2 (reduced Ubiquinone).



In Figure 2, the chemical species and proton are modelled as in § 2.1; the e^- is associated with the *redox potential* of the reaction and can be modelled by an electrical capacitor [11]. Using the Faraday-equivalent potential discussed in § 2.1, the potentials of the chemical species are commensurate with the potentials of the e^- . In particular, under typical cellular conditions (§ 2.2), reaction (11) is associated with a Faraday-equivalent potential Φ of about 345 mV; once again, for this reason the reaction can be used to pump chemical reactions.

2.4 Glycolysis

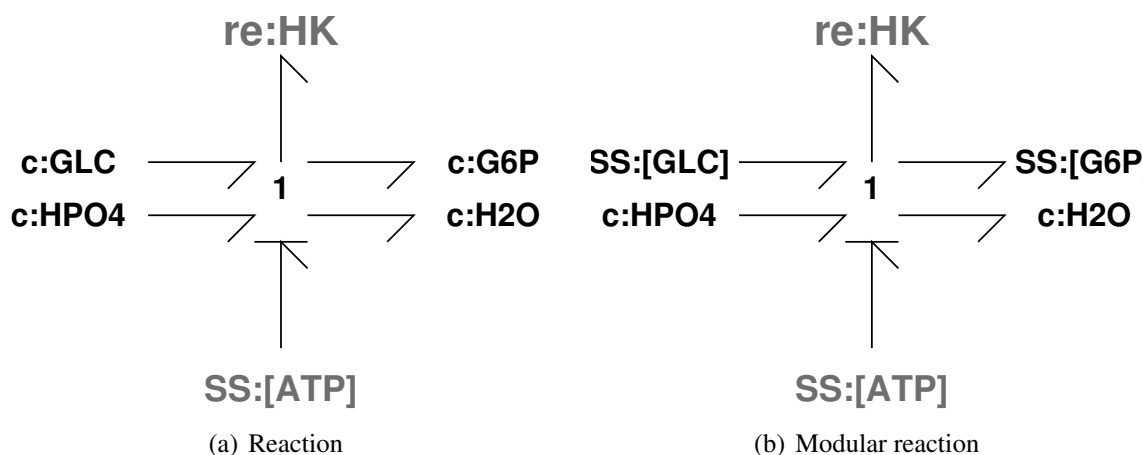
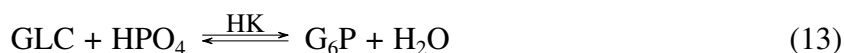


Figure 3: Modularity: hexokinase (HK) reaction

The enzyme hexokinase is involved in a reaction which converts glucose (GLC) to glucose 6-phosphate (G6P):



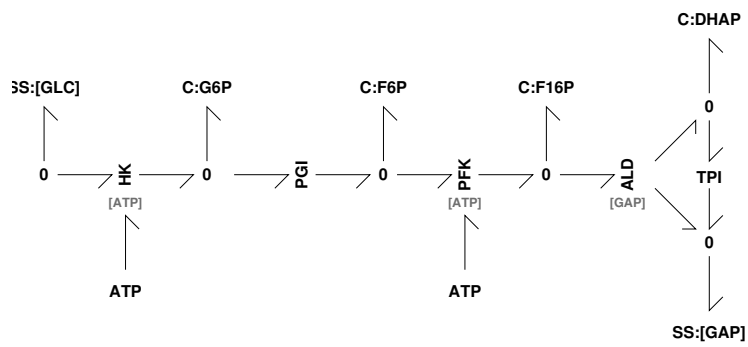
This can be rewritten as the combination of two reactions: ATP hydrolysis reaction (1) and



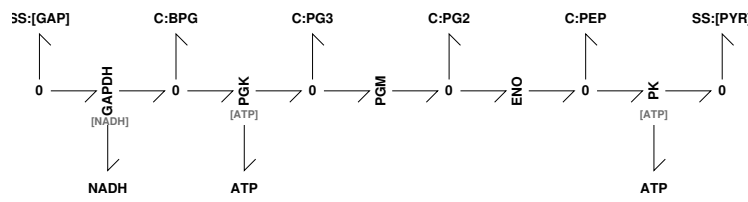
As in § 2.1, the HK reaction (13) has the bond graph representation of Figure 3(a) where the bond graph *source-sensor* component **SS**:**[ATP]** provides a port to connect to the ATP hydrolysis reaction (1). As the HK reaction (13) is to be embedded in a larger model, a modular version is obtained by replacing **C**:**GLC** and **C**:**G6P** by the ports **SS**:**[GLC]** and **SS**:**[G6P]** respectively.

The bond graph models of the two stages of glycolysis are given in Figures 4(a) and 4(b) and are combined in Figure 4(c).

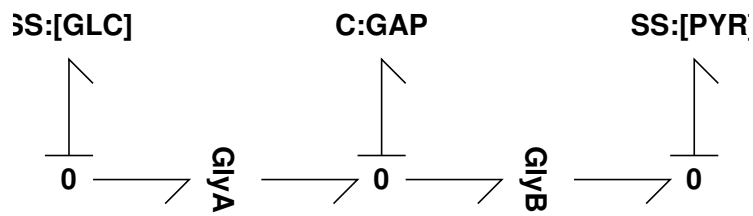
Figure 4(a) shows the modular version of HK embedded in the first stage of glycolysis. This clearly shows the two key features of the HK catalysed reaction: it converts converts GLC to G6P and it is pumped by ATP hydrolysis. In Figure 4(a), the two pathways diverging from the ALD reaction converge on GAP indicate that stage 1 of glycolysis converts each molecule of GLC to two molecules of glyceraldehyde 3-phosphate (GAP) and is pumped by two ATP hydrolysis



(a) GlyA: Stage 1



(b) GlyB: Stage 2

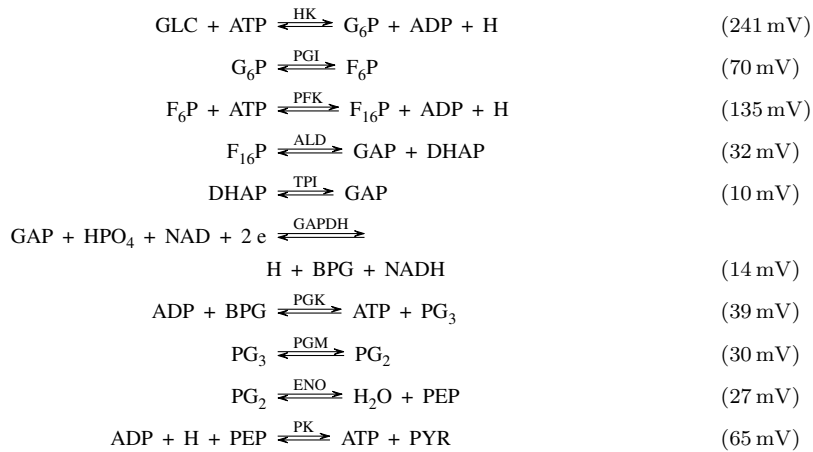


(c) Gly

Figure 4: Glycolysis.

reactions (1). Figure 4(b) shows that stage 2 of glycolysis converts each molecule of GAP to one molecule of PYR and, as indicated by the bond arrow direction, pumps two reverse ATP hydrolysis reactions (1) and a reverse NADH reaction (11).

The modular bond graph of Figure 4 is equivalent to the biomolecular system where the associated reaction potentials Φ correspond to typical cellular conditions (§ 2.2).



3 EFFICIENCY

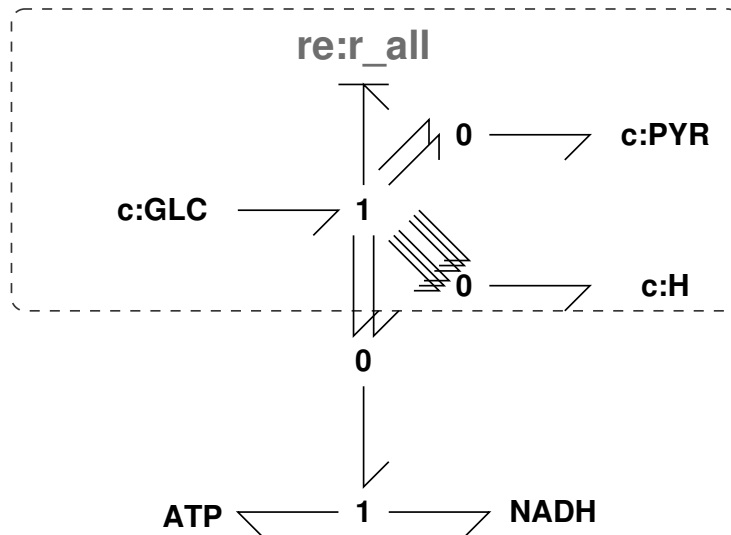


Figure 5: Pumping. The reaction $\text{GLC} \rightleftharpoons 2 \text{PYR} + 6 \text{H}$ pumps the reverse ATP hydrolysis reaction of Figure 1 and the reverse NADH reduction reaction of Figure 2 represented by the modules **ATP** and **NADH** respectively.

The biomolecular network implementing glycolysis discussed in § 2.4 converts glucose (GLC) to pyruvate (PYR) as well as driving ATP hydrolysis and the reduction of NADH in reverse to store chemical energy. In particular, the overall reaction is:



At the standard conditions discussed in § 2.2 and denoted by the \ominus symbol, this reaction is associated with a reaction potential

$$\Phi_{\text{all}}^{\ominus} = 837 \text{ mV} \quad (15)$$

and the corresponding power dissipation is:

$$P_{\text{diss}}^{\ominus} = \Phi_{\text{all}}^{\ominus} f_{\text{PW}} \quad (16)$$

where f_{PW} is the reaction flow rate per unit volume.

As in Figure 5, this reaction can be split into three parts:



The latter two reactions represent two reverse ATP hydrolysis reaction (1) and two reverse NADH reduction reactions (11) respectively; the first reaction represents the remainder of the reaction converting GLC to PYR (and H^+).

The first reaction is associated with a reaction *driving potential*

$$\Phi_0^{\ominus} = \phi_{\text{GLC}}^{\ominus} - 2\phi_{\text{PYR}}^{\ominus} - 6\phi_{\text{H}}^{\ominus} = 2712 \text{ mV} \quad (19)$$

Because the latter two reactions are being pumped by the first, define the *pumping potential* Φ_{pump} as:

$$\begin{aligned} \Phi_{\text{pump}}^{\ominus} &= 2 (\Phi_{\text{ATP}}^{\ominus} + 2\Phi_{\text{NADH}}^{\ominus}) \\ &= 1184 + 690 = 1874 \text{ mV} \end{aligned} \quad (20)$$

These potentials are associated with a corresponding *driving power* P_0 and *pumping power* P_{pump} :

$$P_0 = \Phi_0 f \quad (21)$$

$$P_{\text{pump}} = \Phi_{\text{pump}} f \quad (22)$$

With this example in mind define the *pumping efficiency* as the ratio of pumping power to driving power

$$\begin{aligned} \eta &= \frac{P_{\text{pump}}}{P_0} \\ &= \frac{\Phi_{\text{pump}}}{\Phi_0} \end{aligned} \quad (23)$$

At standard conditions

$$\eta^{\circ} = \frac{\Phi_{pump}^{\circ}}{\Phi_0^{\circ}} = \frac{1874}{2712} = 69.1\% \quad (24)$$

The efficiency computed in Equation (24) corresponds to the nominal values discussed in § 2.2, which in turn correspond to the nominal flow of $f^{\circ} = 2.3$ mM/min. If the concentration of glucose (GLC) is varied, the corresponding potential ϕ_{GLC} varies according to Equation (2). then so will Φ_0 of Equation (19) and the pumping efficiency (23).

$$\eta = \frac{\Phi_{pump}^{\circ}}{\Phi_0^{\circ} + \tilde{\phi}_{GLC}} \quad \text{where } \tilde{\phi}_{GLC} = \Phi_0 - \Phi_0^{\circ} = \phi_{GLC} - \phi_{GLC}^{\circ} \quad (25)$$

Figure 6(a) shows how η varies with $\tilde{\phi}_{GLC}$. Note that $\tilde{\phi}_{GLC} = \Phi_{pump}^{\circ} - \Phi_0^{\circ} = -\Phi_{all}^{\circ}$ corresponds to $\eta = 100\%$. As this value of $\tilde{\phi}_{GLC}$ corresponds to $\Phi_{all}^{\circ} = 0$, the flow $f = 0$ at this point.

Figure 6(b) shows efficiency η plotted against the normalised concentration of GLC.

The computation generating the data for Figure 6 does not involve the Faraday-equivalent flow f . However, efficiency as a function of flow is of interest. As a approximation to this, the steady-state flow f was computed as ϕ_{GLC} was varied assuming that all reactions have the mass-action kinetics of (10) using the method of Gawthrop [34]. This was used to generate the data for Figure 7. In fact, the reaction kinetics are more complicated than the mass-action representation hence the computations are more challenging than those used to generate Figure 7.

These results indicate that, under these particular conditions, the pumping efficiency of glycolysis is around 70% except for very low flow rates associated with low concentrations of Glucose (GLC) and thus Φ_0 being only slightly larger than Φ_{pump} .

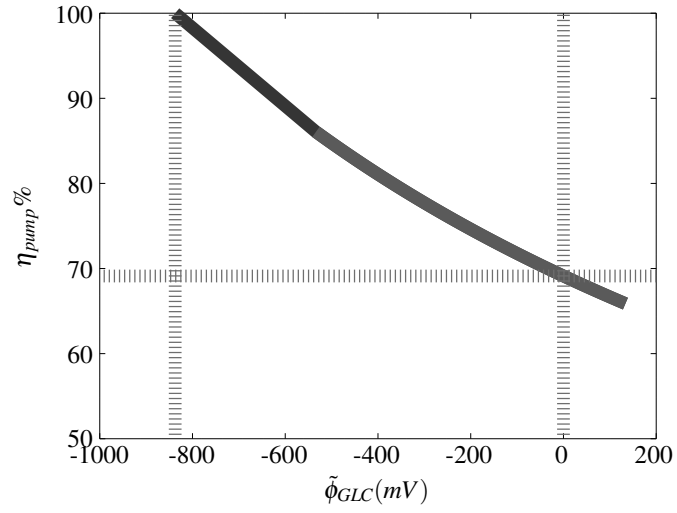
4 CONCLUSION

The basic ideas of modelling biomolecular systems using bond graphs and the Faraday-equivalent potential have been outlined and illustrated using the example of glycolysis: the first stage of aerobic respiration.

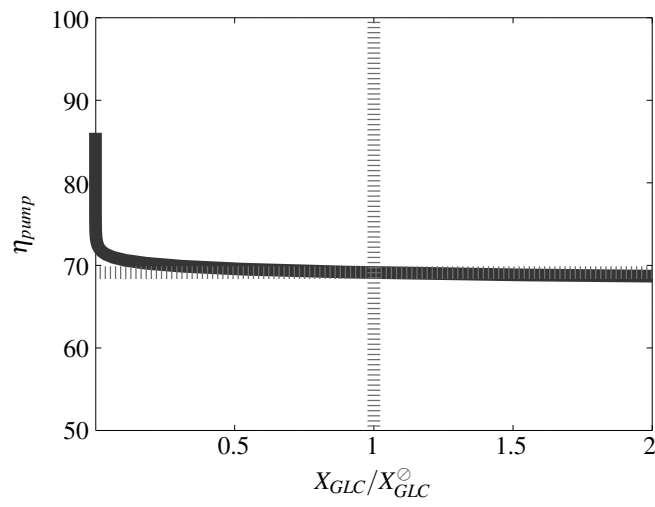
The concept of *pumping efficiency* has been introduced and illustrated using glycolysis and experimental numerical values drawn from the recent paper of Park et al. [22]. These ideas are currently being extended to mitochondrial metabolism: the TCA cycle and the electron transport chain.

References

- [1] Henry M. Paynter. Preface. In J. J. Granda and F. E. Cellier, editors, *Proceedings of the International Conference On Bond Graph Modeling (ICBGM'93)*, volume 25 of *Simulation Series*, page v. Society for Computer Simulation, La Jolla, California, U.S.A., January 1993. ISBN 1-56555-019-6.



(a)



(b)

Figure 6: Pumping Efficiency η_{pump} . Nominal conditions are indicated by the broken lines. (a) Plotted against normalised potential of GLC: $\tilde{\phi}_{GLC}$. (b) Plotted against normalised concentration of GLC.

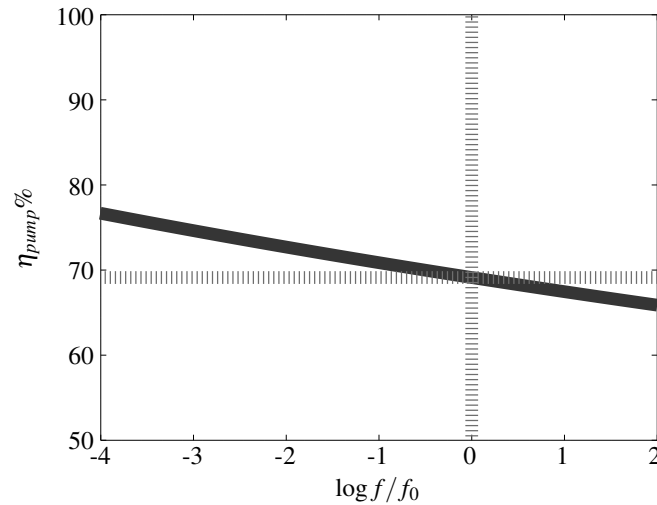


Figure 7: Efficiency η plotted against log normalised flow: $\log_{10} f/f_0$.

- [2] George Oster, Alan Perelson, and Aharon Katchalsky. Network thermodynamics. *Nature*, 234:393–399, December 1971. doi:10.1038/234393a0.
- [3] Dean Karnopp. Bond graph models for electrochemical energy storage : electrical, chemical and thermal effects. *Journal of the Franklin Institute*, 327(6):983 – 992, 1990. ISSN 0016-0032. doi:10.1016/0016-0032(90)90073-R.
- [4] F. E. Cellier. *Continuous system modelling*. Springer-Verlag, 1991.
- [5] Jean U. Thoma and Gianni Mocellin. *Simulation with Entropy Thermodynamics: Understanding Matter and Systems with Bondgraphs*. Springer, 2006. ISBN 978-3-540-32798-1.
- [6] J. Greifeneder and F.E. Cellier. Modeling chemical reactions using bond graphs. In *Proceedings ICBGM12, 10th SCS Intl. Conf. on Bond Graph Modeling and Simulation, Genoa, Italy*, pages 110–121, San Diego, CA, USA, July 2012. The Society for Modeling and Simulation International.
- [7] Peter J. Gawthrop and Edmund J. Crampin. Energy-based analysis of biochemical cycles using bond graphs. *Proceedings of the Royal Society A: Mathematical, Physical and Engineering Science*, 470(2171):1–25, 2014. doi:10.1098/rspa.2014.0459. Available at arXiv:1406.2447.
- [8] P. J. Gawthrop and E. J. Crampin. Modular bond-graph modelling and analysis of biomolecular systems. *IET Systems Biology*, 10(5):187–201, October 2016. ISSN 1751-8849. doi:10.1049/iet-syb.2015.0083. Available at arXiv:1511.06482.
- [9] P. J. Gawthrop, I. Siekmann, T. Kameneva, S. Saha, M. R. Ibbotson, and E. J. Crampin. Bond graph modelling of chemoelectrical energy transduction. *IET Systems Biology*,

- 11(5):127–138, 2017. ISSN 1751-8849. doi:10.1049/iet-syb.2017.0006. Available at arXiv:1512.00956.
- [10] M. Pan, P. J. Gawthrop, K. Tran, J. Cursons, and E. J. Crampin. Bond graph modelling of the cardiac action potential: Implications for drift and non-unique steady states. Submitted., February 2018.
- [11] P. J. Gawthrop. Bond graph modeling of chemiosmotic biomolecular energy transduction. *IEEE Transactions on NanoBioscience*, 16(3):177–188, April 2017. ISSN 1536-1241. doi:10.1109/TNB.2017.2674683. Available at arXiv:1611.04264.
- [12] Peter Sterling and Simon Laughlin. *Principles of neural design*. MIT Press, Cambridge, Massachusetts, 2015. ISBN 978-0-262-02870-7.
- [13] Jeremy E Niven. Neuronal energy consumption: biophysics, efficiency and evolution. *Current Opinion in Neurobiology*, 41:129 – 135, 2016. ISSN 0959-4388. doi:10.1016/j.conb.2016.09.004.
- [14] Stefan Neubauer. The failing heart – an engine out of fuel. *New England Journal of Medicine*, 356(11):1140–1151, 2007. doi:10.1056/NEJMra063052.
- [15] Arnold M Katz. *Physiology of the Heart*. Lippincott Williams and Wilkins, Philadelphia, fifth edition, 2011. ISBN 978-1-60831-171-2.
- [16] Nicholas P. Smith, Christopher J. Barclay, and Denis S. Loiselle. The efficiency of muscle contraction. *Progress in Biophysics and Molecular Biology*, 88(1):1 – 58, 2005. ISSN 0079-6107. doi:10.1016/j.pbiomolbio.2003.11.014.
- [17] Jeremy M. Berg, John L. Tymoczko, Gregory J. Gatto, and Lubert Stryer. *Biochemistry*. W.H. Freeman, eighth edition, 2015. ISBN 1-4641-2910-0.
- [18] Bruce Alberts, Alexander Johnson, Julian Lewis, David Morgan, Martin Raff, Keith Roberts, and Peter Walter., editors. *Molecular Biology of the Cell*. Garland Science, Abingdon, UK, sixth edition, 2015.
- [19] David G Nicholls and Stuart Ferguson. *Bioenergetics 4*. Academic Press, Amsterdam, 2013.
- [20] Jeremy E. Niven and Simon B. Laughlin. Energy limitation as a selective pressure on the evolution of sensory systems. *Journal of Experimental Biology*, 211(11):1792–1804, 2008. ISSN 0022-0949. doi:10.1242/jeb.017574.
- [21] Nick Lane. Bioenergetic constraints on the evolution of complex life. *Cold Spring Harbor Perspectives in Biology*, 6(5), 2014. doi:10.1101/cshperspect.a015982.

- [22] Junyoung O. Park, Sara A. Rubin, Yi-Fan Xu, Daniel Amador-Noguez, Jing Fan, Tomer Shlomi, and Joshua D. Rabinowitz. Metabolite concentrations, fluxes and free energies imply efficient enzyme usage. *Nat Chem Biol*, 12(7):482–489, Jul 2016. ISSN 1552-4450. doi:10.1038/nchembio.2077.
- [23] Daniel S. Lark, Maria J. Torres, Chien-Te Lin, Terence E. Ryan, Ethan J. Anderson, and P. Darrell Neuffer. Direct real-time quantification of mitochondrial oxidative phosphorylation efficiency in permeabilized skeletal muscle myofibers. *American Journal of Physiology - Cell Physiology*, 311(2):C239–C245, 2016. ISSN 0363-6143. doi:10.1152/ajpcell.00124.2016.
- [24] Gary D. Lopaschuk and Naranjan S. Dhalla, editors. *Cardiac Energy Metabolism in Health and Disease*. Springer New York, New York, NY, 2014. ISBN 978-1-4939-1227-8. doi:10.1007/978-1-4939-1227-8.
- [25] D. G. Hardie. AMPK: a key regulator of energy balance in the single cell and the whole organism. *International Journal of Obesity*, 32:S7–S12, 2008. ISSN 0307-0565. doi:10.1038/ijo.2008.116.
- [26] Kenneth Tran, Denis S. Loiselle, and Edmund J. Crampin. Regulation of cardiac cellular bioenergetics: mechanisms and consequences. *Physiological Reports*, 3(7):e12464, 2015. ISSN 2051-817X. doi:10.14814/phy2.12464.
- [27] Stefano Donati, Timur Sander, and Hannes Link. Crosstalk between transcription and metabolism: how much enzyme is enough for a cell? *Wiley Interdisciplinary Reviews: Systems Biology and Medicine*, page e1396, 2017. ISSN 1939-005X. doi:10.1002/wsbm.1396.
- [28] Sunil Nath. The thermodynamic efficiency of ATP synthesis in oxidative phosphorylation. *Biophysical Chemistry*, 219:69 – 74, 2016. ISSN 0301-4622. doi:10.1016/j.bpc.2016.10.002.
- [29] Daniel A. Beard. Simulation of cellular biochemical system kinetics. *Wiley Interdisciplinary Reviews: Systems Biology and Medicine*, 3(2):136–146, 2011. ISSN 1939-005X. doi:10.1002/wsbm.116.
- [30] Jeremy M Berg, John L Tymoczko, and Lubert Stryer. *Biochemistry: international edition*. WH Freeman, New York, seventh edition, 2012. ISBN 978-1-4292-7635-1.
- [31] Peter Atkins and Julio de Paula. *Physical Chemistry for the Life Sciences*. Oxford University Press, 2nd edition, 2011.
- [32] Xin Li, Fan Wu, Feng Qi, and Daniel A. Beard. A database of thermodynamic properties of the reactions of glycolysis, the tricarboxylic acid cycle, and the pentose phosphate pathway. *Database*, 2011:bar005, 2011. doi:10.1093/database/bar005.

- [33] Katja Tummler and Edda Klipp. The discrepancy between data for and expectations on metabolic models: How to match experiments and computational efforts to arrive at quantitative predictions? *Current Opinion in Systems Biology*, 8:1 – 6, 2018. ISSN 2452-3100. doi:10.1016/j.coisb.2017.11.003.
- [34] P. Gawthrop. Computing biomolecular system steady-states. *IEEE Transactions on NanoBioscience*, 17(1):36–43, March 2018. ISSN 1536-1241. doi:10.1109/TNB.2017.2787486. Published online 25th December 2017.